Available online at www.sciencedirect.com
ScienceDirect
Journal of Solid State Chemistry 180 (2007) 2166–2174
JOURNAL OF SOLID STATE CHEMISTRY
www.elsevier.com/locate/jssc

Syntheses, crystal structures, and optical properties of $K_3V_{0.32}Ta_{0.68}S_4$, $K_6Nb_{1.07}Ta_{2.93}S_{22}$, $K_6Nb_{2.97}Ta_{1.03}S_{25}$, $K_3Cu_3Nb_{0.98}Ta_{1.02}S_8$, and $KCu_2Nb_{0.53}Ta_{0.47}S_4$

Yuandong Wu, Wolfgang Bensch*

Institut für Anorganische Chemie, Universität Kiel, Olshausenstr. 40, D-24098 Kiel, Germany

Received 18 December 2006; received in revised form 12 March 2007; accepted 20 May 2007
Available online 26 May 2007

Abstract

The new compounds $K_3V_{0.32}Ta_{0.68}S_4$ (**1**), $K_6Nb_{1.07}Ta_{2.93}S_{22}$ (**2**), $K_6Nb_{2.97}Ta_{1.03}S_{25}$ (**3**), $K_3Cu_3Nb_{0.98}Ta_{1.02}S_8$ (**4**), and $KCu_2Nb_{0.53}Ta_{0.47}S_4$ (**5**) have been synthesized by the reactive flux method. Their crystal structures were determined by single crystal X-ray diffraction. Crystal data: **1**: space group *Pnma*, $a = 9.2354(7)$, $b = 10.6920(6)$, $c = 9.2991(5)$ Å, $Z = 4$; **2**: space group $P2_1/c$, $a = 7.6412(4)$, $b = 8.7572(5)$, $c = 24.5772(14)$ Å, $\beta = 98.559(6)^\circ$, $Z = 2$; **3**: space group $P2_1/n$, $a = 15.7147(10)$, $b = 12.9840(9)$, $c = 18.2363(12)$ Å, $\beta = 104.123(8)^\circ$, $Z = 4$; **4**: space group $C2/c$, $a = 23.5934(19)$, $b = 5.5661(2)$, $c = 14.2373(12)$ Å, $\beta = 120.631(9)^\circ$, $Z = 4$; **5**: space group *Ama*2, $a = 7.4615(4)$, $b = 18.2902(16)$, $c = 5.5320(6)$ Å, $Z = 4$. The structure of compound **1** is based on discrete tetrahedral MS_4 (M = V/Ta) anions, which are separated by K^+ cations. The structure of **2** consists of K^+ cations and $[M_4S_{22}]^{6-}$ (M = Nb/Ta) anions, in which two M_2S_{11} building blocks are linked via terminal sulfur ligands. In **3** the complex anion $[M_4S_{25}]^{6-}$ (M = Nb/Ta) is observed which comprises two M_2S_{11} subunits bridged by a S_3 chain. In **4** $^1_\infty[Cu_3M_2S_8]^{3-}$ (M = Nb/Ta) anionic chains are found which are formed by corner sharing of CuS_4 tetrahedra and edge sharing between CuS_4 and MS_4 tetrahedra. The structure of **5** consists of $[Cu_2MS_4]^-$ (M = Nb/Ta) anionic layers separated by K^+ cations. The CuS_4 and MS_4 tetrahedra share edges and corners yielding layers. All compounds were characterized with Raman spectroscopy and the compound 2–5 with UV/vis diffuse reflectance spectroscopy.
© 2007 Elsevier Inc. All rights reserved.

Keywords: Molten flux method; Group 5 metal polysulfide; Crystal structure; Raman spectrum; UV/vis diffuse reflectance spectroscopy

1. Introduction

During the last two decades, many multinary transition metal chalcogenides were synthesized by applying reactive alkali polychalcogenide fluxes as reaction media at intermediate temperature ($200 \leqslant T \leqslant 500\,^\circ C$) [1,2]. Among these compounds ternary and quaternary sulfides of group 5 elements form a very interesting group. The structures of group 5 ternary sulfides contain isolated tetrahedral MS_4^{3-} units in A_3MS_4 (A = Na, K, Rb, Cs; M = V, Nb, Ta) [3–11], discrete $M_2S_{11}^{4-}$ groups in $A_4M_2S_{11}$ (A = K, Rb, Cs; M = Nb, Ta) [12–16], complex $M_4S_{22}^{6-}$ anions in $A_6M_4S_{22}$ (A = K, Rb, Cs; M = Nb, Ta) [17–21], expanded $M_4S_{25}^{6-}$ units in $A_6M_4S_{25}$ [20,22], and one-dimensional $[NbS_6^-]$ and $[TaS_5^-]$ chains in $NaNbS_6$ [23] and $KTaS_5$ [24], respectively. For the quaternary group 5 sulfides, a variety of compounds with composition $A_2M^IM^VS_4$, $AM_2^IMS_4$, and $A_3M_3^IM_2^VS_8$ (A = K, Rb, Cs; M^I = Cu, Ag; M^V = V, Nb, Ta) [3,25–36] crystallize with low-dimensional anionic building units. The structures of these compounds can be derived from the three dimensionally connected sulvanite-type structure Cu_3VS_4 by successive substitution of the Cu (Ag) atoms by alkali cations.

Solid solutions based on the $K_4Nb_2S_{11}$ structure were successfully prepared via substitutions on the S atom sites (i.e. $K_4Nb_2S_{11-x}Se_x$ [37], $A_4Nb_2S_{10}O$ (A = K, Rb) [38]), and on the alkali atom sites (i.e. $K_4Ba_2(Nb_2S_{11})_2$ [39]). But there are no reports about substitutions of Nb or Ta in this structure type. The two compounds $K_4Nb_2S_{11}$ and

*Corresponding author. Fax: +49 431 880 1520.
E-mail address: wbensch@ac.uni-kiel.de (W. Bensch).

0022-4596/$ - see front matter © 2007 Elsevier Inc. All rights reserved.
doi:10.1016/j.jssc.2007.05.015

$K_4Ta_2S_{11}$ are isostructural adopting the orthorhombic space group $Pca2_1$. Therefore, it should be possible to replace Nb by Ta (or vice versa) yielding the orthorhombic structure type. Interestingly, there is a triclinic modification of $K_4Ta_2S_{11}$ [14], which was not observed for Nb. Another interesting finding is that only one structural modification was reported for $K_6Nb_4S_{22}$ (space group $C2/c$), whereas $K_6Ta_4S_{22}$ is dimorphic and crystallizes in space groups $C2/c$ and $P2_1/c$ under different reaction conditions [17]. A similar observation was made for $A_6M_4S_{25}$. The compound $Rb_6Ta_4S_{25}$ crystallizes in $C2/c$ whereas space group $P2_1/n$ was adopted by $K_6Nb_4S_{25}$. These examples demonstrate the different structural behavior of Nb and Ta sulfides mainly prepared in polysulfide fluxes. After the successive substitution on the Nb sites (i.e. $K_4Nb_{0.96}Ta_{1.04}S_{11}$ [40]), we started to investigate the effect of partial substitution based on K_3TaS_4, $K_6Nb_4S_{22}$, $K_6Nb_4S_{25}$, $K_3Cu_3Nb_2S_8$, and KCu_2NbS_4 structure types. In this paper we report the syntheses, crystal structures, and characterizations of $K_3V_{0.32}Ta_{0.68}S_4$, $K_6Nb_{1.07}Ta_{2.93}S_{22}$, $K_6Nb_{2.97}Ta_{1.03}S_{25}$, $K_3Cu_3Nb_{0.98}Ta_{1.02}S_8$, and $KCu_2Nb_{0.53}Ta_{0.47}S_4$.

2. Experimental

2.1. Reagents

The following reagents were used as obtained unless noted: (i) K metal, 99.95%, ABCR GmbH & Co.KG; (ii) S, 99.99%, Heraeus; (iii) Nb powder, 99.8%, 325 mesh, Alfa Aesar; (iv) Ta powder, 99.98%, 325 mesh, ABCR GmbH & Co.KG; (v) Cu powder, 99.5%, 200 mesh, Alfa Aesar; (vi) V powder, 99.7%, 325 mesh, Heraeus.

2.2. Synthesis

The compound K_2S_3 was prepared from the reaction of stoichiometric amounts of elemental K and S powder in liquid ammonia under an argon atmosphere.

$K_3V_{0.32}Ta_{0.68}S_4$ (**1**): K_2S_3, V, Ta, and S in a 4/2/1/8 molar ratio were thoroughly mixed in a nitrogen-filled glove box. The mixture was then loaded into a glass ampoule (Duran®), which was subsequently evacuated ($\sim 2\times10^{-3}$ mbar) and flame sealed. The ampoule was heated from 25 to 500 °C in 24 h and kept at this temperature for 6 days, cooled to 100 °C at a rate of 2 °C/h followed by cooling to room temperature in 4 h. The resulting black melt was washed with DMF and acetone and the product was dried in vacuum. The product consists of black platelet crystals (yield ~50%). The crystals are stable in dry air for several weeks, but decompose slowly under humid conditions. An EDX analysis of single crystals indicated the presence of all four elements (K, V, Ta, S) in an approximate atomic ratio of 9:1:2:12.

$K_6Nb_{1.07}Ta_{2.93}S_{22}$ (**2**): The preparation and isolation process of **2** were similar to those of **1**. However, the mixture of K_2S_3, Nb, Ta, S (molar ratio: 3:1:3:14) was heated at 450 °C for 6 days in a glass ampoule (Duran®). After cooling with 2 °C/h, transparent red platelets were obtained in a yield of about 90%. The compound is stable in dry air for several weeks. An EDX analysis of single crystals indicated the presence of all four elements (K, Nb, Ta, S) in an atomic ratio of 6:1:3:22.

$K_6Nb_{2.97}Ta_{1.03}S_{25}$ (**3**): The procedure for the synthesis of **3** is the same as that for **2** except that the molar ratio was changed to 3:3:1:14. The melt contained red polyhedral crystals in a 90% yield. The crystals are stable in dry air for several weeks. The EDX analysis of selected single crystals indicated the presence of all four elements (K, Nb, Ta, S) in an atomic ratio of 6:3:1:25.

$K_3Cu_3Nb_{0.98}Ta_{1.02}S_8$ (**4**) and $KCu_2Nb_{0.53}Ta_{0.47}S_4$ (**5**): Crystals were prepared by reacting a mixture of K_2S_3, Cu, Nb, Ta, S with a molar ratio of 2:4:1:1:7. After being sealed in a silica tube under vacuum ($\sim 2\times10^{-3}$ mbar), the starting material was heated to 600 °C, held there for 6 days, and cooled down to 100 °C at a rate of 2 °C/h, followed by cooling to room temperature in 4 h. After removing excess K_2S_x flux with DMF followed by washing with acetone, transparent brown needles (**4**: 40%) and transparent green needles (**5**: 40%) were obtained. Both compounds are stable in dry air for several months. The EDX analyses of single crystals indicated the presence of all five elements (K, Cu, Nb, Ta, S) in an atomic ratio of 3:3:1:1:8 for compound **4** and 2:4:1:1:8 for compound **5**.

2.3. X-ray crystallography

All single crystal X-ray investigations were performed using an imaging plate diffraction system (IPDS) (Mo$K\alpha$-radiation; $\lambda = 0.71073$ Å) equipped with a low-temperature device from Oxford Cryosystem. The crystals were mounted on top of glass fibers and bathed in cold nitrogen stream during data collection. The raw intensities were treated in the normal way applying Lorentz, polarization, and numerical absorption corrections. All structures were solved with direct methods using SHELXS-97 and refined against F_o^2 using SHELXL-97 of Shelxtl program package [41].

On the basis of the systematic absences the space groups $Pnma$ for **1**, $P2_1/c$ for **2**, $P2_1/n$ for **3**, $C2/c$ for **4**, and $Ama2$ for **5** were chosen. After successful assignments of the high electron density peaks as Ta, (Cu), K, and S atoms, the displacement parameters and occupancy on each atomic site were examined. For all compounds the S atom sites are fully occupied with reasonable displacement parameters. The refined occupancies of heavy metal sites, initially assigned to Ta, were significantly low indicating that lighter atoms V or Nb are also involved in this site. Therefore, disorder models were applied by introducing V or Nb atoms so that the sum of the occupancies were set equal to full occupancy to maintain charge balance. The other sites were found suitable for K atoms and/or Cu atoms based on the observed electron densities. After successive

refinements of the positional parameters and site occupation factors (SOF) of all atom sites, reasonable displacement parameters for all atoms were obtained, as well as low residual electron densities. The final formulae were refined as $K_3V_{0.32(1)}Ta_{0.68(1)}S_4$ for **1**, $K_6Nb_{1.07(1)}Ta_{2.93(1)}S_{22}$ for **2**, $K_6Nb_{2.97(1)}Ta_{1.03(1)}S_{25}$ for **3**, $K_3Cu_3Nb_{0.98(1)}Ta_{1.02(1)}S_8$ for **4**, and $KCu_2Nb_{0.53(1)}Ta_{0.47(1)}S_4$ for **5**. The SOFs of V/Ta or Nb/Ta show a ratio near 1:2 in compounds **1**, **2**, and **3**, and 1:1 in compounds **4**, **5**, which may indicate a certain kind of ordering. Long exposed images gave no hints for superstructures.

Technical details of the data acquisition as well as some refinement results are summarized in Table 1.

Further details of the crystal structure investigation can be ordered referring to the No CSD-417842 ($K_3V_{0.32(1)}Ta_{0.68(1)}S_4$), CSD-417843 ($K_6Nb_{1.07(1)}Ta_{2.93(1)}S_{22}$), CSD-417844 ($K_6Nb_{2.97(1)}Ta_{1.03(1)}S_{25}$), CSD-417841 ($K_3Cu_3Nb_{0.98(1)}Ta_{1.02(1)}S_8$), CSD-417845 ($KCu_2Nb_{0.53(1)}Ta_{0.47(1)}S_4$), the authors and the citation of this paper at the Fachinformationszentrum Karlsruhe, Gesellschaft für wissenschaftlich-technische Information mbH. D-76344 Eggenstein-Leopoldshafen (Germany). E-mail: crysdata@fiz-karlsruhe.de

2.4. Physical measurements

Raman spectroscopy: Raman spectra were collected on an ISF-66 spectrometer (Bruker) with additional FRA 106 Raman module. A Nd/YAG laser was used as the source of excitation ($\lambda = 1064$ nm). The samples were ground and prepared on Al sample holders. The measuring range was from -1000 to 3500 cm^{-1} with a resolution of 2 cm^{-1}.

Solid-state UV/vis/NIR spectroscopy: Spectra were recorded on a Cary 5 spectrometer (Varian Techtron Pty.). The spectrometer was equipped with an Ulbricht sphere (Diffuse reflectance accessory; Varian Techtron Pty.). The inner wall of the Ulbricht sphere (diameter 110 mm) was covered with a PTFE layer of 4 mm thickness. A PbS detector (NIR) and a photomultiplier (UV/vis) were attached to the Ulbricht sphere.

The samples were ground together with $BaSO_4$ and prepared as a flat specimen of approximate 2 mm thickness. Resolution was 1 nm for the UV/vis range and 2 nm for the near-IR range. The measuring range was 250–2000 nm. $BaSO_4$ was used as white standard for 100% reflectance. Absorption data were calculated from the reflectance data

Table 1
Technical details of data acquisition and some refinement results

Compound	**1**	**2**	**3**	**4**	**5**
Formula	$K_3V_{0.32}Ta_{0.68}S_4$	$K_6Nb_{1.07}Ta_{2.93}S_{22}$	$K_6Nb_{2.97}Ta_{1.03}S_{25}$	$K_3Cu_3Nb_{0.98}Ta_{1.02}S_8$	$KCu_2Nb_{0.53}Ta_{0.47}S_4$
Crystal system	Orthorhombic	Monoclinic	Monoclinic	Monoclinic	Orthorhombic
Space group	*Pnma*	$P2_1/c$	$P2_1/n$	$C2/c$	*Ama*2
a (Å)	5.2354(7)	7.6412(4)	15.7147(10)	23.5934(19)	7.4615(4)
b (Å)	10.6920(6)	8.7572(5)	12.9840(9)	5.5661(2)	18.2902(16)
c (Å)	9.2991(5)	24.5753(14)	18.2363(12)	14.2373(12)	5.5320(6)
β (deg)	–	98.559(6)	104.123(8)	120.631(9)	–
V (Å)	918.24(10)	1626.2(2)	3608.5(4)	1608.8(2)	754.96(11)
Z	4	2	4	4	4
T (K)	170	293	293	170	170
Calcd. den. ($g\,cm^{-3}$)	2.785	3.205	2.759	3.467	3.780
μ Mo (mm^{-1})	10.674	12.375	6.184	13.253	14.842
$F(0\,0\,0)$	713	1448	2944	1546	789
2θ range (deg)	$6^\circ \leqslant 2\theta \leqslant 56^\circ$	$5^\circ \leqslant 2\theta \leqslant 56^\circ$	$5^\circ \leqslant 2\theta \leqslant 56^\circ$	$6^\circ \leqslant 2\theta \leqslant 56^\circ$	$7^\circ \leqslant 2\theta \leqslant 56^\circ$
Index range	$-12 \leqslant h \leqslant 12$	$-8 \leqslant h \leqslant 10$	$-20 \leqslant h \leqslant 20$	$-30 \leqslant h \leqslant 30$	$-10 \leqslant h \leqslant 10$
	$-14 \leqslant k \leqslant 13$	$-11 \leqslant k \leqslant 11$	$-17 \leqslant k \leqslant 17$	$-7 \leqslant k \leqslant 6$	$-25 \leqslant k \leqslant 25$
	$-12 \leqslant l \leqslant 12$	$-32 \leqslant l \leqslant 32$	$-23 \leqslant l \leqslant 24$	$-18 \leqslant l \leqslant 18$	$-7 \leqslant l \leqslant 7$
Indep. refl.	1170	3900	8549	1908	1184
Refl. [$F_o > 4\sigma(F_o)$]	1128	3353	7199	1805	1143
R_{int}	0.0438	0.0322	0.0503	0.0291	0.0360
Min/max. transm.	0.1499/0.3231	0.1576/0.2172	0.3416/0.4631	0.1279/0.2292	0.1278/0.1858
No. of parameters	45	148	321	77	47
a^*	0.0577	0.0438	0.0600	0.0579	0.0689
b^*	3.9	0	22.1	4.8	0
R_1 for $F_o > 4\sigma(F_o)$	0.0330	0.0269	0.0417	0.0296	0.0332
wR_2 for all data	0.0894	0.0621	0.1113	0.0802	0.0970
GooF	1.120	0.992	1.034	1.077	1.201
Flack parameter x	–	–	–	–	−0.09(3)
$\Delta\rho$($e Å^{-3}$)	1.596/−2.073	1.092/−1.689	5.359/−1.893	2.311/−1.668	1.964/−1.862

$R_1 = \Sigma||F_o|-|F_c||/\Sigma|F_o|$.
w$R_2 = [\Sigma w(F_o^2-F_c^2)^2/\Sigma w(F_o^2)^2]^{1/2}$, $w = 1/[\sigma(F_o^2) + (a^*P)^2 + b^*P]$,
where $P = (\max(F_o^2,0) + 2F_c^2)/3$.

using the Kubelka–Munk function [42]. The approximate band gap was determined as the intersection point between the energy axis and the line extrapolated from the linear part of the absorption edge in a $(F(R))^2$ vs. energy plot.

3. Results and discussion

3.1. Crystal structure

The crystal structure of $K_3V_{0.32}Ta_{0.68}S_4$ (**1**) is shown in Fig. 1. $K_3V_{0.32}Ta_{0.68}S_4$ is isostructural to the A_3MQ_4 family of compounds, where $A = K$, Rb, Cs; $M = V$, Nb, Ta; $Q = S$, Se [3–11]. It is built from the packing of MS_4^{3-} ($M = V/Ta$) anions and K^+ cations. The M (V/Ta) atom is tetrahedrally coordinated, and the M–S distances (2.2269(13) to 2.2394(16) Å) are somewhat smaller than those in K_3TaS_4 [10] and longer than in K_3VS_4 [3] due to the partial substitution of Ta by V. The S–M–S angles (108.58(6) to 111.77(7)°) are close to the tetrahedral value (109.47°). The two crystallographically independent K^+ ions are coordinated by seven S atoms in an irregular polyhedron (cutoff for K–S distances: 4.0 Å). K(1) is linked to four symmetry-related MS_4 tetrahedra whereas K(2) is connected to five. The distances for K(1)–S and K(2)–S range from 3.196(2) to 3.515(2) Å (average 3.319(2) Å) and from 3.121(2) to 3.736 Å (average 3.430(2) Å), respectively. These distances are also shorter than those in K_3TaS_4 [10].

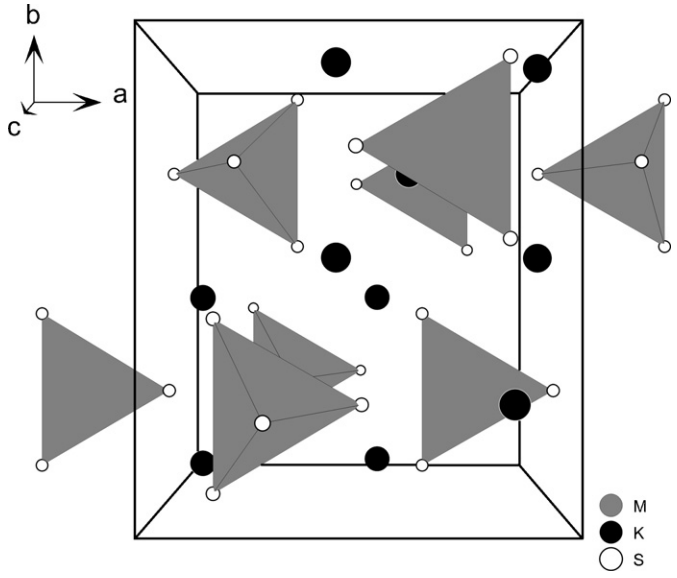

Fig. 1. Crystal structure of $K_3V_{0.32}Ta_{0.68}S_4$ (**1**) with perspective view along [0 0 1].

In the structure of $K_6Nb_{1.07}Ta_{2.93}S_{22}$ (**2**) which is isostructural to the second modification of $K_6Ta_4S_{22}$ [17], discrete $[M_4S_{22}]^{6-}$ anions and K^+ cations are found (Fig. 2). Each $[M_4S_{22}]^{6-}$ anion is composed of two M_2S_{11} building blocks linked via terminal sulfur ligands. The coordination mode of $[M_4S_{22}]^{6-}$ (Fig. 3) can be described as $[(M_2(\mu{-}\eta^2, \eta^1{-}S_2)_3(\eta^2{-}S_2)(S)_2)_2(\mu{-}\eta^1{-}S_2)]^{6-}$. Within the $[M_4S_{22}]^{6-}$ anion, each nonbonding M pair (M–M distance 3.5499(3) Å) is bridged by three S_2^{2-} ligands with an average M–S distance of 2.471(2) Å and S–S bonds of 2.087(2) Å. Each M atom is bound to a terminal S anion to form a relatively short M–S bond (average: 2.237(2) Å). The coordination sphere of the M atoms is completed by the addition of two S_2^{2-} ligands (S–S distance = 2.090(2) Å) per M pair. One S_2^{2-} ligand is bound to an M atom in a typical η^2–fashion while the second S_2^{2-} links the other M atom to a neighboring dimer yielding a tetrameric anion with M in the +5 oxidation state. The M–S distances, M–M separation, and S–S bond lengths are nearly identical to those of $K_6Ta_4S_{22}$ (II) [17].

The structure of $K_6Nb_{2.97}Ta_{1.03}S_{25}$ (**3**) consists of K^+ cations and $[M_4S_{25}]^{6-}$ (M = Nb/Ta) anions (Fig. 4), and is

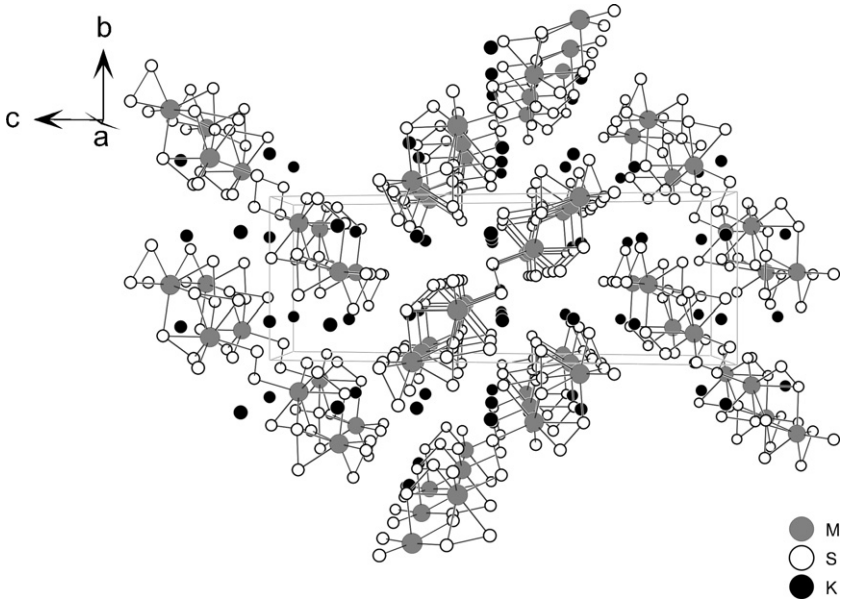

Fig. 2. Crystal structure of $K_6Nb_{1.07}Ta_{2.93}S_{22}$ (**2**) with perspective view along [1 0 0].

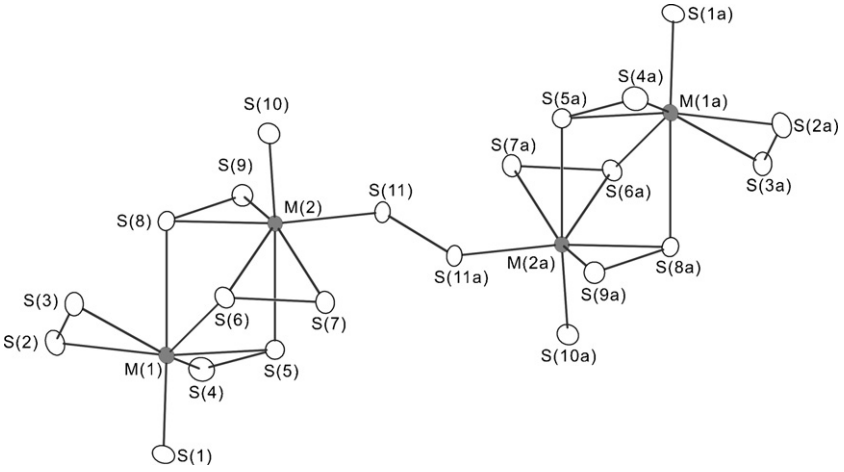

Fig. 3. $[M_4S_{22}]$ units in the structure of $K_6Nb_{1.07}Ta_{2.93}S_{22}$ (**2**) with atomic labeling. The ellipsoids are drawn at the 50% probability level.

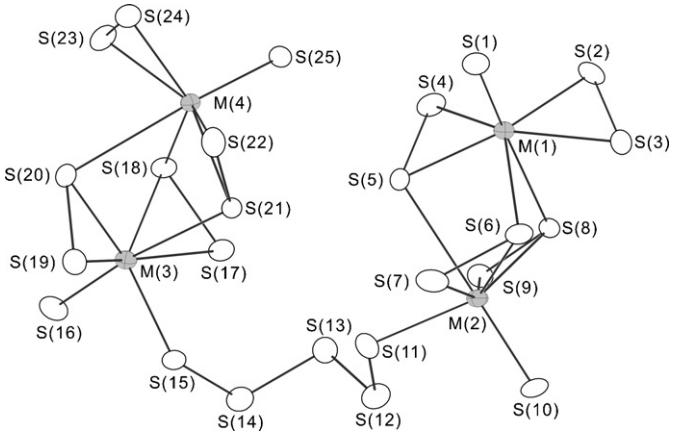

Fig. 4. $[M_4S_{25}]$ units in the structure of $K_6Nb_{2.97}Ta_{1.03}S_{25}$ (**3**) with atomic labeling. The ellipsoids are drawn at the 50% probability level.

isostructural to $K_6Nb_4S_{25}$ [22]. One anion is composed of two M_2S_{11} subunits, which are connected by a S_3 chain. The coordination mode of the resulting $[M_4S_{25}]^{6-}$ anion can be described as $[(M_2(\mu_2{-}\eta^2,\eta^1{-}S_2)_3(\eta^2{-}S_2)(S)_2)_2(\mu_2{-}\eta^1,\eta^1{-}S_5)]^{6-}$. Each M atom has a short bond to the axial S^{2-} (S(1) and S(10)) of about 2.2 Å. Five M–S separations scatter around 2.4 Å, and finally a long interatomic M–S distance of about 2.9 Å is observed to a S atom of a η^2–S_2^{2-} anion attached to the neighbored M atom. The long M–S distances are always in *trans* position to the short M–S bonds (Fig. 4). The M–S distances match well with those reported for $K_6Nb_4S_{25}$ [22] and $Rb_6Ta_4S_{25}$ [20]. The S–S bonds in the S_2^{2-} anions are between 2.036(2) and 2.099(2) Å (average 2.072 Å), typical for S–S single bonds. The shortest M–M distance amounts to 3.574(2) Å, which is too long for significant metal to metal interactions. The angles S–S–S in the S_5^{2-} anion vary between 107.1(1)° and 108.8(1)° and are near the expected tetrahedral angles.

The six crystallographically independent K^+ ions are coordinated by 9 or 11 S atoms with K–S distances varying from 3.083(2) to 3.794(2) Å. The average K–S separations (3.322–3.479 Å) match well with the sum of the ionic radii of K^+ and S^{2-}.

$K_3Cu_3Nb_{0.98}Ta_{1.02}S_8$ (**4**) is isostructural to $K_3Cu_3M_2S_8$ (M = Nb, Ta) [30] and the structure is composed of anionic chains $^1_\infty[Cu_3M_2S_8]^{3-}$ (M = Nb/Ta) being separated by K^+ ions (Fig. 5). The chains are directed along [0 1 0] (Fig. 6) with the shortest interchain separation of 3.632(1) Å between S(4) atoms of adjacent chains. Within the chains the unique M atom and the two independent Cu atoms are tetrahedrally coordinated by S atoms. The MS_4 and $Cu(2)S_4$ tetrahedra share common edges along [0 1 0] to form the infinite one-dimensional $[CuMS_4]$ chains. Two adjacent chains are interconnected by $Cu(1)S_4$ tetrahedra in such way that the $Cu(1)S_4$ tetrahedra have common edges with MS_4 tetrahedra along [1 0 0] and common corners with $Cu(2)S_4$ tetrahedra. Since there are no S–S interactions the formal oxidation states K(+1), Cu(+1), M(+5), and S(−2) can be assigned. Similar copper—group 5 metal—chalcogen chains were found previously in $K_3Cu_3M_2S_8$ (M = Nb, Ta) [30]. The mean Cu–S distances are longer than the analogous bonds in $K_3Cu_3Nb_2S_8$ whereas the mean M–S bond lengths are almost the same as those in $K_3Cu_3Nb_2S_8$.

The compound $KCu_2Nb_{0.53}Ta_{0.47}S_4$ (**5**) crystallizes isostructural to KCu_2NbS_4 [31] (Fig. 7). It is composed of two-dimensional $[Cu_2MS_4]^-$ layers, which are parallel to the (0 1 0) plane and K^+ ions located between the layers. The shortest interlayer S–S distance of 3.776(1) Å is longer than the sum of the van der Waals radii of S. Obviously there are no interactions between the adjacent layers. Within the $[Cu_2MS_4]^-$ layers (Fig. 8), M and Cu atoms are tetrahedrally coordinated by S atoms. Alternating MS_4 and $Cu(1)S_4$ tetrahedra share common edges to form $[Cu(1)MS_4]$ chains along [0 0 1], like the one-dimensional chains in K_2CuNbS_4 [25]. The $Cu(2)S_4$ tetrahedra share common corners with the $Cu(1)S_4$ tetrahedra along [1 0 0] and have common edges with MS_4 tetrahedra along [1 0 0]. This connection mode yields the $\mathbf{[}Cu_2MS_4\mathbf{]}^-$ layers. The M–S bond lengths (2.283(2)–2.335(3) Å) match well with

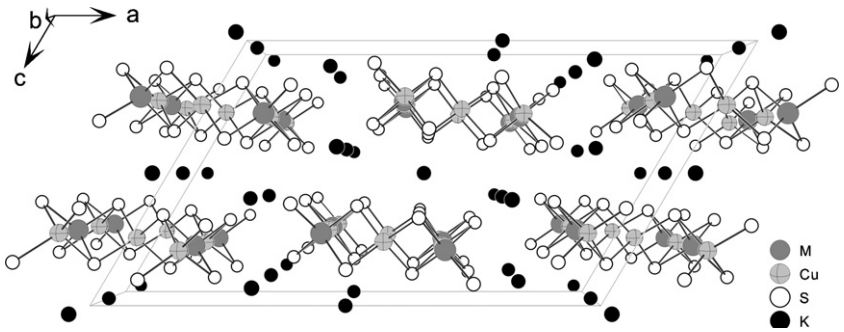

Fig. 5. Crystal structure of $K_3Cu_3Nb_{0.98}Ta_{1.02}S_8$ (**4**).

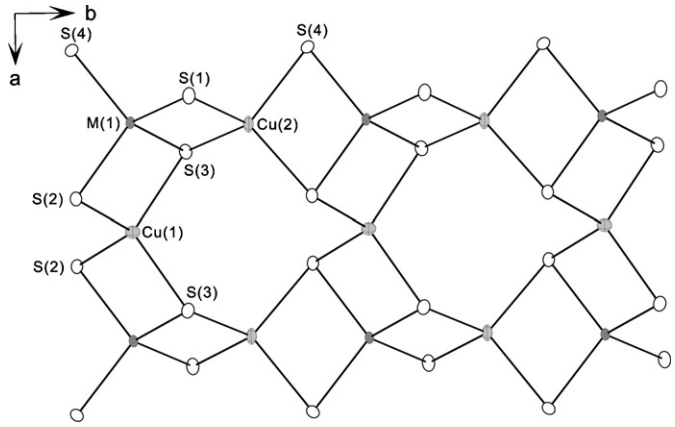

Fig. 6. $[Cu_3M_2S_8]^{3-}$ chain in the structure of $K_3Cu_3Nb_{0.98}Ta_{1.02}S_8$ (**4**) with atomic labeling. The ellipsoids are drawn at the 50% probability level.

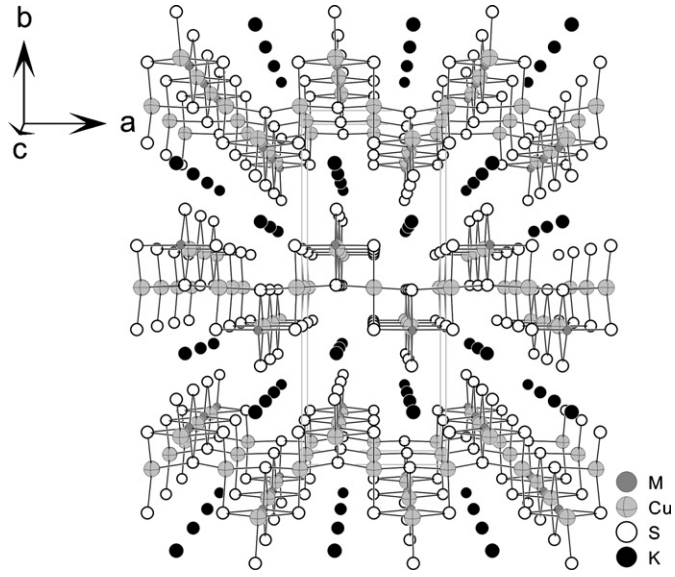

Fig. 7. Perspective view of the structure of $KCu_2Nb_{0.53}Ta_{0.47}S_4$ (**5**) along [0 0 1].

those in compound **4**. The S–M–S angles vary from 107.61(5)° to 112.38(6)°, close to the normal tetrahedral values. The Cu–S bonds from 2.334(2) to 2.359(2) Å are slightly shorter than the Cu–S distances (2.346(2)–2.372(2) Å) in **4**. The S–Cu–S angles about the two crystallographically independent Cu atoms are different. The S–Cu(1)–S angles are close to the normal tetrahedral value (105.66(6)–113.01(5)°), while the S–Cu(2)–S angles scatter from 104.85(5)° to 117.29(6)°, which clearly indicates the stronger distortion of the $Cu(2)S_4$ tetrahedron. The K^+ ions are coordinated by nine S atoms choosing a cutoff of 4.0 Å for the K–S distances. The K–S distances range from 3.400(3) to 3.778(1) Å (average: 3.564(2) Å). The formal oxidation states of all atoms in this compound can be assigned as K(+1), Cu(+1), M(+5), and S(−2).

3.2. Optical properties

The FT-Raman spectra of $K_3V_{0.32}Nb_{0.68}S_4$ (**1**) in the range 100–550 cm^{-1} are shown in Fig. 9. The Raman spectrum shows shifts at 486, 468, 445, 405, 205, 183, and 133 cm^{-1}. The energy shifts at 486, 468, 445, and 405 cm^{-1} can be assigned to M–S stretching vibrations, whereas vibrations at 205, 183, and 133 cm^{-1} are related to the S–M–S deformation modes of MS_4 tetrahedra. Due to the shorter M–S bond length (2.227(1) Å), the stretching vibration are located at higher energy compared to the data of Tl_3TaS_4 (Ta–S: 2.35 Å) [43].

Fig. 10 shows the FT-Raman spectrum of $K_6Nb_{1.07}Ta_{2.93}S_{22}$ (2). It displays resonances at 508, 466, 449, 435, 344, 304, 289, 278, 255, 235, 202, 181, 166, 147, 136, 116, and 94 cm^{-1}. Unfortunately, no Raman data were reported for $A_6M_4S_{22}$ (A = K, Rb, Cs; M = Nb, Ta), and the effect of partial substitution cannot be directly compared. Compared with the Raman spectrum of $K_4Ba_2(Nb_2S_{11})_2$ [39], the spectrum of 2 is more complex. The S–S stretching mode (ν(S–S)) of the disulfide ligands at 508 cm^{-1} with a shoulder at lower energy is the most intense band. For $K_2Ta_2S_{10}$ [24], the ν(S–S) mode occurs at 511 and 505 cm^{-1} supporting the assignment. The peaks at 466, 449, and 435 cm^{-1} are due to symmetric ν_s(M–S) stretching vibrations of the terminal sulfide ions. In the Raman spectrum of $K_4Ba_2(Nb_2S_{11})_2$ this mode shows a bathochromic shift. The difference of the energetic position of this band may be due to the presence of Nb/Ta in compound 2. The bands at 344, 304 cm^{-1} are assigned to the symmetric $\nu_s(M–S_\mu)$ stretching mode of M–S–M

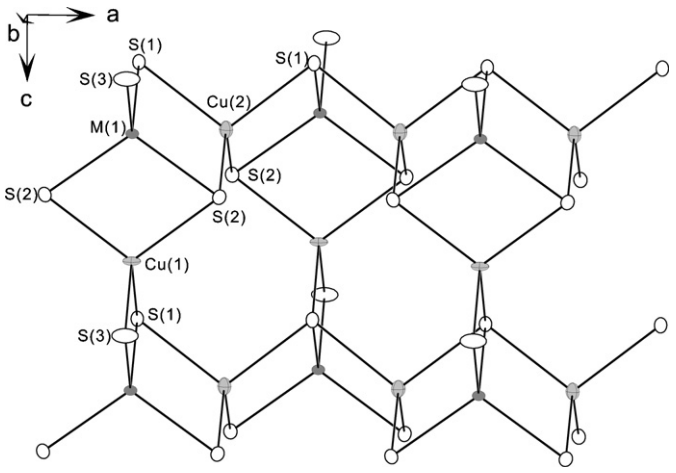

Fig. 8. Part of the $[Cu_2MS_4]^-$ layer in the structure of $KCu_2Nb_{0.53}Ta_{0.47}S_4$ (**5**) with atomic labeling. The ellipsoids are drawn at the 50% probability level.

bridges whereas the bands at 289, 278, 255, 235 cm^{-1} are due to the mixed M–S vibrations. The peaks below 202 cm^{-1} may be caused by S–M–S bending or deformation modes.

In the Raman spectrum three resonances are observed at 512, 494, 474, 464, 441, 353, 329, 295, 272, 245, 218, 192, 176, 150, 131, 116, and 105 cm^{-1} (Fig. 11). The $\nu_s(M–S_t)$ stretching vibration at 474 cm^{-1} is the most intense band. The S–S stretching vibrations occur at 512, 494 cm^{-1}, the M–S vibrations at 353–218 cm^{-1}, and S–M–S deformation modes below 200 cm^{-1}.

The FT-Raman spectrum of $K_3Cu_3Nb_{0.98}Ta_{1.02}S_8$ (**4**) is displayed in Fig. 12. The Raman spectrum shows shifts at 456, 445, 425, 415, 264, 232, 194, 139, 109, and 93 cm^{-1}. In accordance to our previous work [31], the resonances at 456, 425, and 415 cm^{-1} may be assigned to M–S symmetric stretching vibrations, the peak at 445 cm^{-1} to an asymmetric mode. The shifts at 264, 232, and 194 cm^{-1} can be

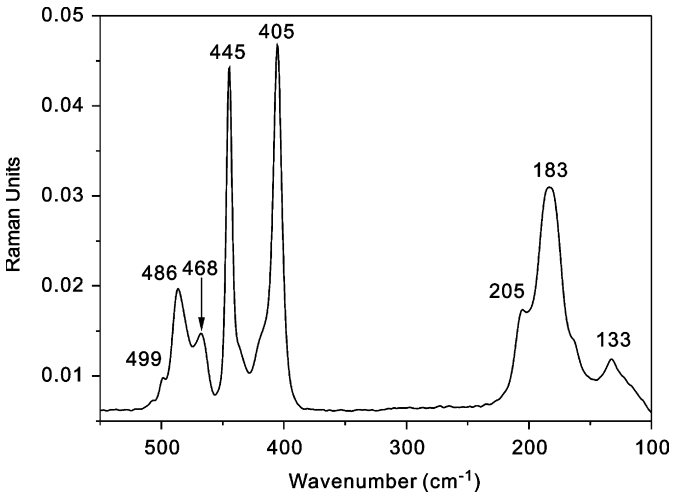

Fig. 9. Raman spectra of $K_3V_{0.32}Ta_{0.68}S_4$ (**1**).

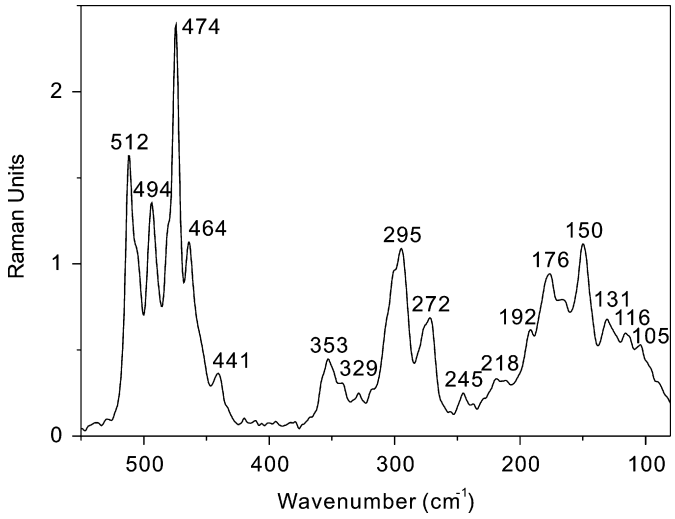

Fig. 11. Raman spectrum of $K_6Nb_{2.97}Ta_{1.03}S_{25}$ (**3**).

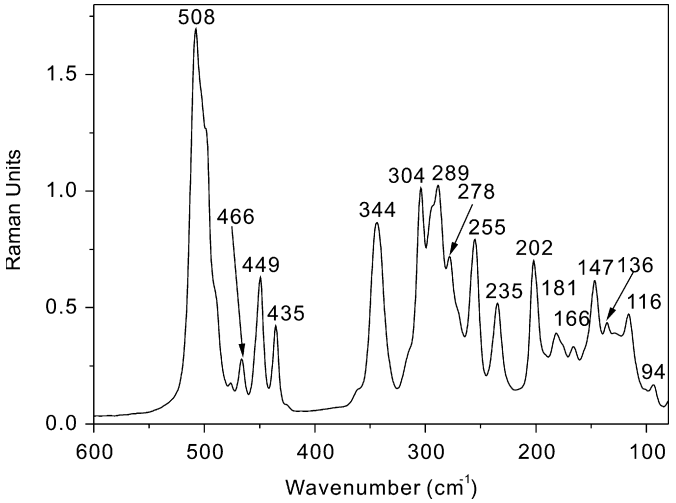

Fig. 10. Raman spectrum of $K_6Nb_{1.07}Ta_{2.93}S_{22}$ (**2**).

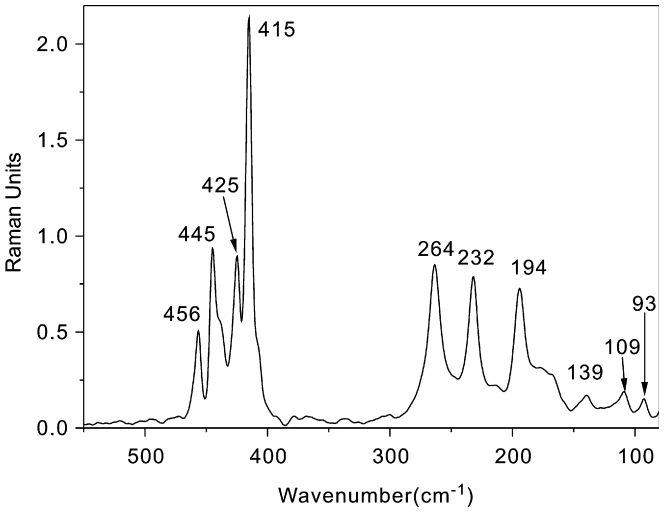

Fig. 12. Raman spectra of $K_3Cu_3Nb_{0.98}Ta_{1.02}S_8$ (**4**).

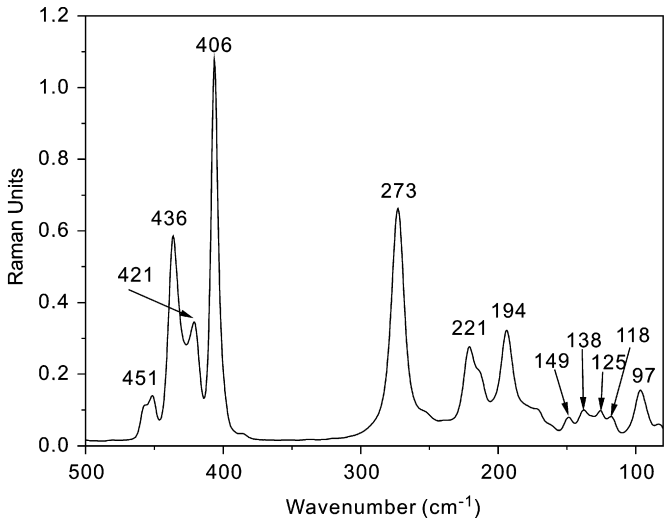

Fig. 13. Raman spectra of $KCu_2Nb_{0.53}Ta_{0.47}S_4$ (**5**).

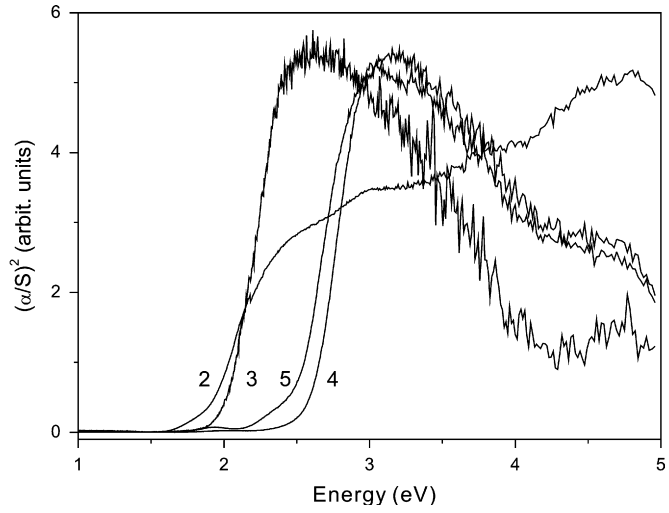

Fig. 14. Transformed reflectance spectra of compounds **2–5**.

assigned to the Cu–S valence vibrations and S–M(Cu)–S deformation modes, respectively. The assignment of peaks at lower energy is still not clear.

In the Raman spectrum of $KCu_2Nb_{0.53}Ta_{0.47}S_4$ (**5**), resonances at 451, 436, 421, 406, 273, 221, 194, 149, 138, 125, 118, and 97 cm^{-1} are seen (Fig. 13). The patterns are very similar to those of compound **4** allowing an identical assignment of the different modes (see above).

The compounds 2–5 exhibit well-defined electronic absorption spectra with sharp optical absorption edges associated with energy gaps of 1.88 eV for compound 2, 2.01 eV for compound 3, 2.61 eV for compound 4, and 2.50 eV for compound 5 (Fig. 14). The optical absorptions are likely due to charge-transfer transitions from filled S-based *p*-orbitals to empty M-based orbitals. Compared to available data for $A_4Ta_4S_{22}$ (A = K, Rb) ($E_g = 2.21$ eV) and $Rb_6Ta_4S_{25}$ ($E_g = 2.35$ eV) [44], the simultaneous presence of Nb and Ta in the structures of compounds 2 and 3 decreases the band gap by about 0.3 eV.

In conclusion, five compounds $K_3V_{0.32}Ta_{0.68}S_4$ (**1**), $K_6Nb_{1.07}Ta_{2.93}S_{22}$ (**2**), $K_6Nb_{2.97}Ta_{1.03}S_{25}$ (**3**), $K_3Cu_3Nb_{0.98}Ta_{1.02}S_8$ (**4**), and $KCu_2Nb_{0.53}Nb_{0.47}S_4$ (**5**) have been synthesized under different conditions. The mixed compound $K_6Nb_{1.07}Ta_{2.93}S_{22}$ crystallizes in space group $P2_1/c$, a modification that was only observed for the pure Ta compound. In $K_6Nb_{2.97}Ta_{1.03}S_{25}$ the Nb content seems to determine the actual structure type and the material adopts space group $P2_1/n$, which was also reported for the pure Nb sample in contrast to the pure Ta compound crystallizing in $C2/c$.

Attempts to synthesize new compounds with different V/Nb, V/Ta, and Nb/Ta ratios were unsuccessful except the presented examples **1–5** and $K_4Nb_{0.96}Ta_{1.04}S_{11}$ [39]. During the syntheses the ratios of the transition metals in the flux were varied over a large range. According to EDX analyses, the final products contained the metals in ratios very close to that given in the manuscript. Interestingly, compound 1 could only be obtained applying a large S excess. We cannot exclude that compounds with different metal atom ratios can be prepared changing for instance the reaction temperature. In many cases the Rb and Cs analogs of K-containing compounds were reported. But all attempts to prepare analogous Rb and Cs compounds were not successful.

Acknowledgments

Financial support by the State of Schleswig-Holstein, the Fonds der Chemischen Industrie (FCI), and DFG (Deutsche Forschungsgemeinschaft) is gratefully acknowledged.

Appendix A. Supplementary materials

Supplementary data associated with this article can be found in the online version at doi:10.1016/j.jssc.2007.05.015.

References

[1] M.G. Kanatzidis, Chem. Mater. 2 (1990) 353–363.
[2] M.G. Kanatzidis, A.C. Sutorik, Prog. Inorg. Chem. 43 (1995) 151–265.
[3] P. Dürichen, W. Bensch, Eur. J. Solid State Inorg. Chem. 33 (1996) 309–320.
[4] M. Emirdag-Eanes, J.A. Ibers, Z. Kristallogr.—NCS 216 (2001) 489–490.
[5] K.O. Klepp, G. Gabl, Eur. J. Solid State Inorg. Chem. 34 (1997) 1143–1154.
[6] R. Niewa, G.V. Vajenine, F.J. DiSalvo, J. Solid State Chem. 139 (1998) 404–411.
[7] M. Latroche, J.A. Ibers, Inorg. Chem. 29 (1990) 1503–1505.
[8] O. Krause, C. Näther, I. Jess, W. Bensch, Acta Crystallogr. C 54 (1998) 902–904.

[9] S. Herzog, C. Näther, P. Dürichen, W. Bensch, Z. Anorg. Allg. Chem. 624 (1998) 2021–2024.
[10] S. Herzog, C. Näther, W. Bensch, Acta Crystallogr. C 54 (1998) 1742–1744.
[11] B. Deng, J.A. Ibers, Acta Crystallogr. E 60 (2004) i147–i148.
[12] W. Bensch, P. Dürichen, Eur. J. Solid State Inorg. Chem. 33 (1996) 527–536.
[13] K.O. Klepp, G. Gabl, Z. Naturforsch. 53b (1998) 1236–1238.
[14] S. Herzog, C. Näther, W. Bensch, Z. Anorg. Allg. Chem. 625 (1999) 969–974.
[15] S. Schreiner, L.E. Aleandri, D. Kang, J.A. Ibers, Inorg. Chem. 28 (1989) 392–393.
[16] P. Dürichen, W. Bensch, Acta Crystallogr. C 54 (1998) 706–708.
[17] P. Stoll, C. Näther, W. Bensch, Z. Anorg. Allg. Chem. 628 (2002) 2489–2494.
[18] W. Bensch, P. Dürichen, Z. Anorg. Allg. Chem. 622 (1996) 1963–1967.
[19] P. Stoll, C. Näther, I. Jess, W. Bensch, Z. Anorg. Allg. Chem. 626 (2000) 959–962.
[20] P. Stoll, C. Näther, I. Jess, W. Bensch, Solid State Sci. 2 (2000) 563–568.
[21] P. Stoll, C. Näther, I. Jess, W. Bensch, Acta Crystallogr. C 56 (2000) e368–e369.
[22] W. Bensch, P. Dürichen, Eur. J. Solid State Inorg. Chem. 33 (1996) 1233–1240.
[23] W. Bensch, C. Näther, P. Dürichen, Angew. Chem. 37 (1998) 133–135.
[24] Y. -D. Wu, C. Näther, W. Bensch, J. Solid State Chem. 178 (2005) 1569–1574.
[25] W. Bensch, P. Dürichen, C. Weidlich, Z. Kristallogr. 211 (1996), 933–933.
[26] K. Peters, E.-M. Peters, H.G. von Schnering, C. Mujica, G. Carvajal, J. Llanos, Z. Kristallogr. 211 (1996), 812–812.
[27] R. Tillinski, C. Näther, W. Bensch, Acta Crystallogr. C57 (2001) 333–334.
[28] C. Rumpf, R. Tillinski, C. Näther, P. Dürichen, I. Jess, W. Bensch, Eur. J. Solid State Inorg. Chem. 34 (1997) 1187–1198.
[29] W. Bensch, P. Dürichen, C. Weidlich, Z. Kristallogr. 211 (1996), 931–931.
[30] Y.-J. Lu, J.A. Ibers, J. Solid State Chem. 98 (1992) 312–317.
[31] Y.-J. Lu, J.A. Ibers, J. Solid State Chem. 94 (1991) 381–385.
[32] Y.-D. Wu, C. Näther, W. Bensch, Z. Naterforsch. 59b (2004) 1006–1014.
[33] W. Bensch, P. Dürichen, Chem. Ber. 129 (1996) 1207–1210.
[34] R. Tillinski, C. Rumpf, C. Näther, P. Dürichen, I. Jess, S.A. Schunk, W. Bensch, Z. Anorg. Allg. Chem. 624 (1998) 1285–1290.
[35] W.-T. Chen, H.-W. Ma, G.-C. Guo, L. Deng, G.-W. Zhou, Z.-C. Dong, J.-S. Huang, Bull. Chem. Soc. Jpn. 77 (2004) 505–509.
[36] K.O. Klepp, G. Gabl, Eur. J. Solid State Inorg. Chem. 34 (1997) 1119–1131.
[37] O. Krause, P. Dürichen, C. Näther, W. Bensch, Solid State Sci. 2 (2000) 197–203.
[38] O. Krause, P. Dürichen, C. Näther, W. Bensch, Eur. J. Solid State Inorg. Chem. (1999) 1295–1299.
[39] Y.-D. Wu, C. Näther, N. Lehnert, W. Bensch, Solid State Sci. 7 (2005) 1062–1069.
[40] Y.-D. Wu, C. Näther, W. Bensch, Acta Crystallogr. E. 61 (2005) i208–i210.
[41] A. Bruker, SHELXTL Version 5.1, Bruker AXS Inc. Madison, Wisconsin, USA, 1998.
[42] P. Kubelka, F. Munk, Z. Tech. Phys. 12 (1931) 593–601.
[43] K.H. Schmidt, A. Müller, J. Bouwma, F. Jellinek, J. Mol. Struct. 11 (1972) 275–282.
[44] P. Stoll, Ph.D. Dissertation, University Kiel, 2002.